Morpho-elasticity of human pluripotent stem cell cysts

Joseph Ackermann, Philippe J.R. Cohen, Kevin Alessandri, Andrea Leonard, Pierre Nassoy, Jean-François Joanny, Martine Ben Amar

A morpho-elastic framework of growing self-organized cysts of human pluripotent stem cells for guiding stem cell bioprocessing

Joseph Ackermann,[1] Philippe J.R. Cohen,[2,3] Kevin Alessandri,[3] Andrea Leonard,[3] Pierre Nassoy,[4,5] Jean-François Joanny,[6,7] and Martine Ben Amar[8,9,*]

[1] *Laboratoire de Physique de l'Ecole normale supérieure , ENS , Université PSL, CNRS Sorbonne Université Université de Paris, F-75005, Paris, France*
[2] *Imagine Institute iPSC Core Facility, Université de Paris, INSERM, France*
[3] *Treefrog Therapeutics, F-33600, Pessac, France*
[4] *LP2N Laboratoire Photonique Numérique et Nanosciences, Univ. Bordeaux, F-33400, Talence France*
[5] *Institut d'Optique Graduate School, CNRS UMR 5298, F-33400, Talence, France*
[6] *Collège de France, 11 place Marcelin Berthelot, 75231 Paris Cedex 05, France*
[7] *Physico-Chimie Curie, Institut Curie, CNRS UMR 168, PSL University, Sorbonne Université, 26 rue d'Ulm, F-75248, Cedex 05, France*
[8] *Laboratoire de Physique de l'Ecole normale supérieure , ENS , Université PSL, CNRS Sorbonne Université Université de Paris, F-75005, Paris,France*
[9] *Institut Universitaire de Cancérologie Faculté de médecine Sorbonne Université 91 Bd de l'Hôpital F-75013 Paris France*

Human pluripotent stem cells (hPSCs) are a promising cellular source in cell therapies or regenerative medicine and they allow to address fundamental mechanisms in embryo-genesis. However, their culture to provide large amounts of high quality stem cells remains challenging. Here, using an encapsulation microfluidic device, we observe that hPSCs self-organize into cysts, which are spherical closed epithelia reminiscent of the early stages of *in vitro* embryo models. We monitor their morphology, organization and growth in a pseudo-stratified epithelia before and after they get confined by the capsule wall. Then, we present a morpho-elastic model to quantitatively explain the growth dynamics. The model based on Neo-Hookean elasticity with anisotropic growth shows that the stresses, concentrated within the cyst, remain at a low level. Cyst growth is shown to be quasi-exponential, hardly reduced by a compression-induced correction. We hypothesize that this peculiar morphological dynamics, which is controlled by elasticity and anisotropic growth, might provide new strategies to optimize the production of medical grade hPSCs.

INTRODUCTION

Human pluripotent stem cells (hPSCs) have emerged as the most promising cellular source for cell therapies, organ engineering or drug testing, because of the possibility to reprogram terminally differentiated cells into human induced pluripotent cells (hiPSCs) [1], which are then capable of expanding infinitely before differentiation on demand. While differentiation protocols towards mature phenotypes have been recently improved, one of the greatest bottlenecks for biomedical applications remains upstream: the culture and expansion of hPSCs to clinically-relevant numbers.

Typically 10^6-10^{10} cells are required for stem cells derived therapies. The standard method for cell expansion relies on 2D tissue culture. Not only is the expansion rate limited by the surface area of the flasks, but also by laborious tasks of replating and colony selection that lead to inherent heterogeneity and lack of reproductibility. Better, less time-consuming and more cost-effective scalability can be achieved with suspension culture systems such as microcarriers [2] or aggregates in stirred bioreactors [3]. Embedded single cells, cell aggregates or cell-on-microcarriers in a gel allow for further improvements, especially to protect the cells against shear forces at play in agitated cultures [4]. In all cases, pluripotency markers are conserved and although the expansion rate depends on the method (scaffold versus suspension, nature of the scaffold), on the initial cell density, on the seeding strategy (single cell versus clusters) and on the composition of the culture medium, hiPSCs expansion results in the formation and growth of spheroids that ultimately reach a maximal size of about 300 µm, corresponding to the limit above which oxygen and nutrient diffusion restriction leads to the formation of necrotic cores.

In parallel, in a completely different context, hPSCs have been used to generate high-grade stem cell-derived organoids [5] and to investigate *in vitro* the self-organization programs that are executed in the embryo *in vivo* [6]. Several works have shown that pluripotent stem cells self-organize into cysts reminiscent of the lumenal epiblast stage [7]. Starting from a two-cell assembly [8] or with a single hPSC with a perinuclear apicosome structure [9], hPSCs seem to be programmed to form lumen and thus cysts upon growth.

At the onset of this work, we found puzzling that 3D cultures of pluripotent stem cells are reported to form aggregates (i.e plain spheroids, without lumen) [3, 4, 10] when tissue engineering and regenerative medicine applications are aimed, while they readily self-organize in polarized cysts in developmental biology oriented works for apparently similar conditions. We have recently developed a microfluidic technique that allows to grow and differentiate pluripotent stem cells in permeable micro-compartments or capsules with micro-engineered extracellular matrix-like environment, see Refs. [11, 12]. Its high throughput capability makes the approach *a priori* compatible with a massive production required in regenerative medicine. However, since

all micro-compartments can be handled and monitored individually, we have also investigated the morphology within individual capsules and monitored the growth of 3D hiPSCs cultures from an initially small cell density (between 1 and 10 cells). Here, we show that 3D cells of hiPSCs indeed start growing as cysts that further become pseudostratified epithelia closed around a lumen. Since it is now recognized that mechanical cues are important regulators of the self-organization and fate of tissues [5], we investigated the mechanics of this peculiar morphodynamical growth. We propose a simple morpho-elastic model to account for the radial expansion of the cyst and the thickening of the epithelium. The dynamics is critically tested and validated at all times, even at post-confluence where elastic boundaries are modified by the contact with the capsule. These findings suggest that bioprocessing conditions recapitulating hPSC self-organization as cysts that grow under reduced mechanical stress could be a new route to explore for more effective cell amplification.

Results

HiPSCs encapsulation

We encapsulated a suspension of hiPSCs in hollow alginate spheres, referred to as capsules, following a protocol previously reported [12]. Briefly, we used a 3D-printed microfluidic device to generate a composite co-extrusion flow : the cell suspension is injected in the inner capillary and is surrounded by an alginate solution that flows into the outer channel. Both solutions are separated by a neutral sorbitol solution to prevent calcium diffusion from the cell suspension to the alginate solution and cause chip plugging. On exiting the nozzle, the Rayleigh-Plateau instability fragments the coaxial flow into composite droplets. In this jetting regime, the droplet radius is set by the diameter of the nozzle (around $150\,\mu$m). When the droplets fall into a 100 mM calcium bath, the alginate undergoes rapid gelation, and cells are entrapped in hollow capsules (*Fig. 1a*). Since hiPSCs are sensitive to anoikis and that native alginate is cell-repellent, we introduced Matrigel into the gel suspension. As reported previously [12] , liquid Matrigel crosslinks in warm (37°C) calcium bath, forming a few micrometers thick layer interconnected with the alginate inner wall to which hiPSCs may adhere. We used low encapsulation densities, in the order of 4×10^5 cells/mL in the cell-Matrigel suspension so that the number of cells per capsule upon encapsulation is kept low, but sufficient to promote proliferation, typically below 10 cells. The capsules were then transferred to mTSER1 medium and placed into the incubator for one day before monitoring by video-microscopy.

Growth stages of encapsulated hiPSC cysts

Using phase contrast imaging, we observed that hiPSCs, which were encapsulated within individual capsules, readily self-organize as a cyst in 3D around a central lumen. We could then monitor their growth over a period of almost two weeks on a temperature - and atmosphere - controlled microscope stage. Representative snapshots of cyst growth are displayed in Figure 1c (see also Movie S1). Three main regimes are observed. First, as long as the cyst is smaller than the capsule, in a stage referred to as pre-confluence, the hiPSC cyst grows freely and conserves its spherical shape and gets thicker by contrast with cysts of epithelial cell lines like MDCK cells [13]. When the cyst starts to contact the capsule, it follows the shape of the capsule, which always exhibits some deviation from sphericity. Nonetheless, in the rest of this work, we will assume that the shape remains spherical and will characterize its size with an effective radius derived from the measured cross-section. The second stage corresponds to confluence, when the cyst is fully constrained by the internal wall of the shell, corresponding to the confluent stage. Finally, in the post-confluent stage, the cyst is compressed by the elastic capsule and mostly grows inwards until contrast between the lumen and the epithelium is lost, suggesting that a lumen-free aggregate is formed.

Cellular organization, pluripotency of the growing cysts

We first checked whether hiPSC cysts grow as monolayers. In the pre-confluent stage, we fixed cysts and performed nuclear and actin immunostaining. Since actin is mostly localized in the sub-membrane cortex, phalloidin staining allows to delineate cell contours. Figure 1b shows that cysts are indeed organized as a pseudo-stratified columnar epithelium, where, although the nuclei are found at different positions, all cells bridge the apical pole and the basal membrane. Then, we performed staining against two main pluripotency markers, namely SOX2 and OCT4. In the post-confluent stage, where external mechanical forces are at play and could impact cell differentiation [14] , we observed that all cells remain SOX2 and OCT4 positive, indicating that pluripotency is conserved throughout cyst growth course.

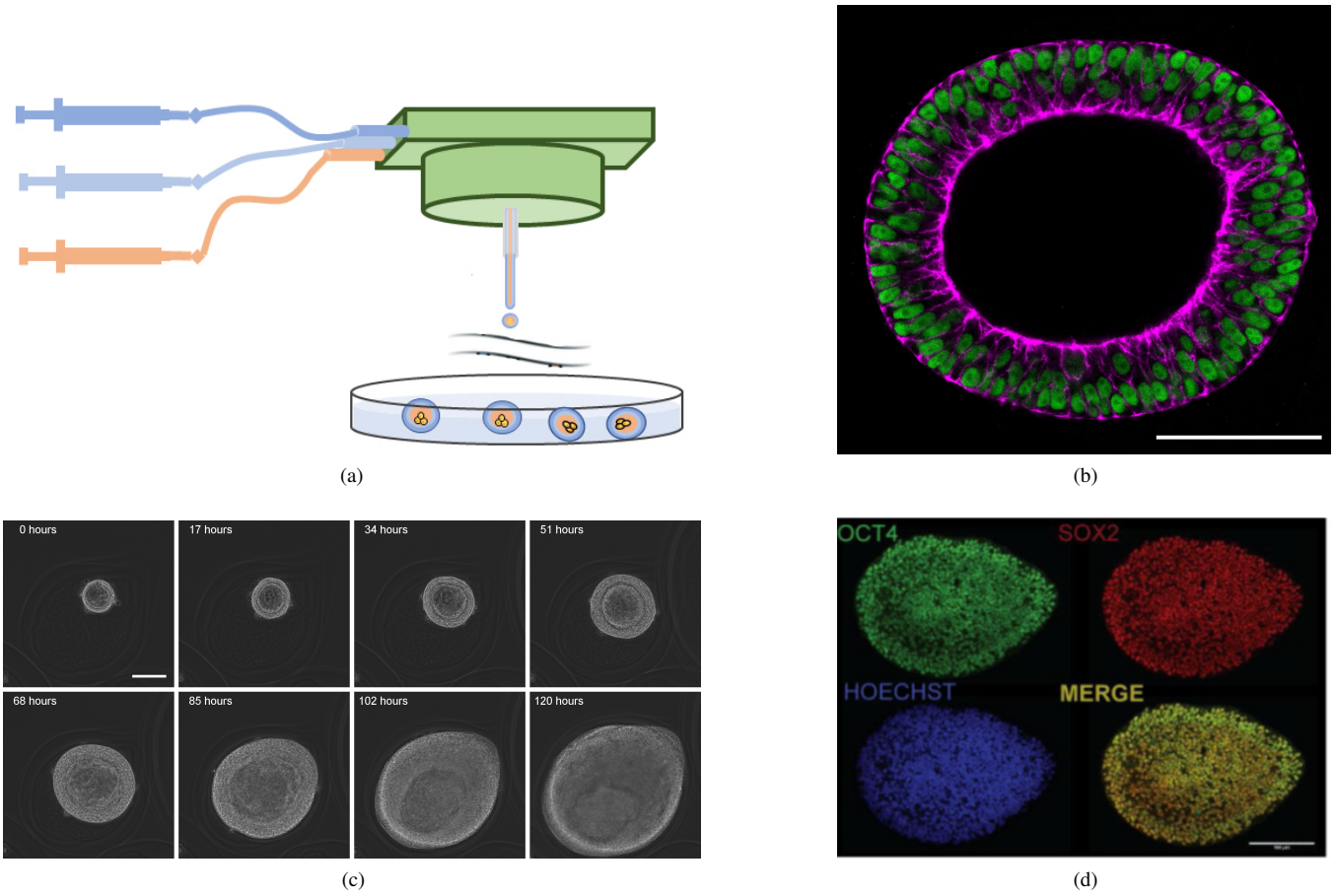

(a) (b) (c) (d)

FIG. 1: **Growth, morphological and stemness characterization of encapsulated hiPSC cysts. (a) :** *Drawing of the microfluidic encapsulation platform. The three solutions (alginate solution in dark blue, sorbitol solution in light blue, and hiPSC/Matrigel mixture in orange) are injected simultaneously by computer-controlled syringes into a 3D-printed device (in green). The composite droplets formed upon Rayleigh instability fall into a calcium bath and form the hollow capsules entrapping the cells.* **(b) :** *Confocal image of the equatorial plane of a cyst stained for nucleus (DAPI in green) and actin (phalloidin in magenta). scale bar is* $100\,\mu$m. **(c) :** *Snapshots of hiPSC cysts growing inside an alginate capsule. Time interval between images is* $17\,$h *and scale bar is equal to* $100\,\mu$m. **(d) :** *Confocal images of encapsulated hiPSC colonies in the late stages (*~ 10 *days after encapsulation) stained for two standard stemness markers (OCT4 and SOX2) and nucleus (HOECHST).*

Monitoring the morpho-dynamics of hiPSCs cyst growth

Figure 2a displays a typical kymograph of a cyst over a period of 7 days. The lumen, the epithelium and the alginate shell are clearly visible. In particular, 3D confluence can be detected from the deformation of the shell, which occurs simultaneously in both sides of the line scan. After confluence, the thickness of the cyst increases more drastically. We have mentioned above that in later stages (not seen here), the lumen even vanishes. However, even in the pre-confluent stages, the cyst thickens while it grows, which is consistent with the picture of a growing pseudo-stratified epithelium. In order to provide a mechanistic explanation of this growth dynamics, we quantitatively measured the external and internal radii of the cysts, r_o and r_i, from the measured cross-section after image segmentation. Figures 2b-c show representative curves of the variations of r_i, r_o and the cyst thickness h as a function of time. For the sake of clarity, we applied a time offset to all curves so that confluence corresponds to $t = 7\,$days. Although the initial size of the cyst and of the capsule may slightly differ from one capsule to another, the overall dynamics followed over an extended period of time (around 2 weeks) exhibits robust similarities. Starting from an initial radius of $r_o \sim 50\,\mu$m and a thickness of $h \sim 15\,\mu$m, confluence is reached for $r_o \sim 150\,\mu$m after $7 - 10\,$days.

At this last stage, the cyst has already reached a thickness of about $50\,\mu$m, indicating that cells are significantly stretched to span both sides of the epithelium. From confluence on, cyst growth is slowed down due to elastic confinement by a hydrogel shell whose Young's modulus is $E_{alg} \sim 68\,$kPa [11] and the cyst thickening drastically increases, leading potentially to a closure of the lumen. Although these observations may explain why 3D cell cultures of hiPSCs sometimes lead to cysts or to aggregates,

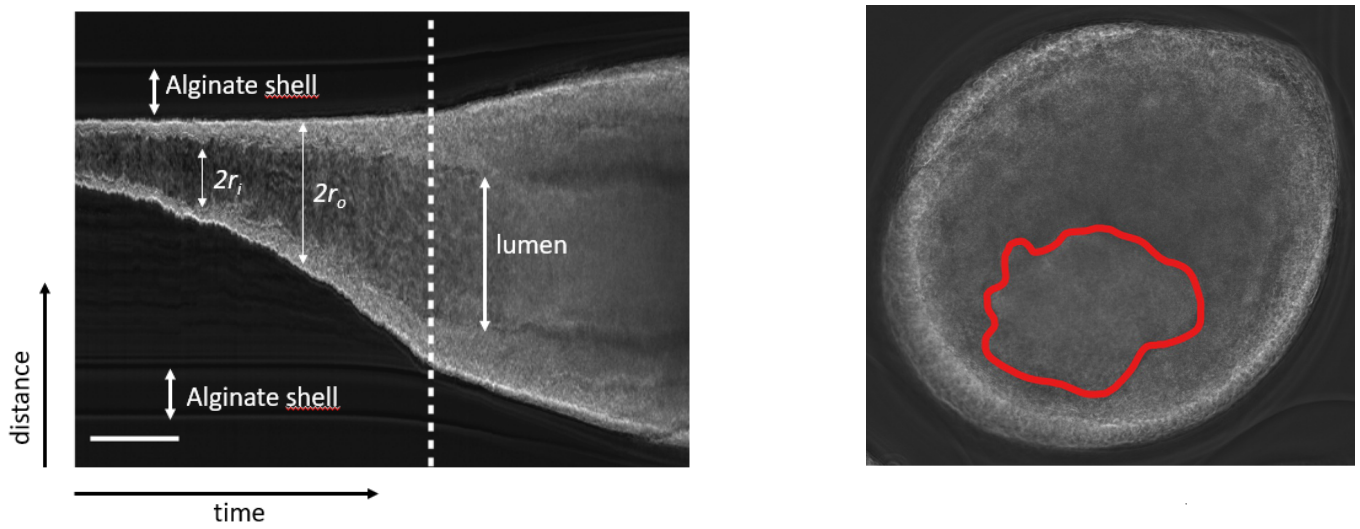

(a) (b)

FIG. 2: **Morphological evolution of encapsulated growing cysts. (a)** : *Kymograph distance versus time through an encapsulated hiPSC cyst (notations defined in the main text). The dotted line represents the time at which confluence is reached. The scale bar corresponds to* 1 *day for the abscissa axis and to* 100 *µm for the ordinate axis.* **(b)** : *Image of a Biot instability at the interface between the cells and the lumen. The contour of the instability is underlined in red.*

depending on the time scale at which they are considered, we were further intrigued by this peculiar morpho-dynamical evolution.

Growth and elasticity of cysts

We propose here a theoretical description of the cyst growth inside an alginate capsule, which couples the growth to the mechanical stresses in the cyst and the capsule. This model, adapted from a previous work by one of us [15] calculates the growth of a spherical cyst with a central lumen at discrete times with the assumption that the mechanical forces equilibrate at each step.

Growth model and morpho-elasticity of shells

We assume that during the process, only elasticity and cell proliferation regulate the dynamics of the cyst expansion. In morpho-elasticity, growth is represented by a symmetric second order tensor, with 3 eigen-values in 3 orthogonal directions. At a given time t, in each of these directions, the eigen-value γ_i represents the deformation gradient due to growth in the direction i with respect to the reference state at time $t = 0$. If the spherical symmetry of the cyst is preserved during growth, the 3 eigen-directions are the radial direction r and the two angular directions θ and ϕ which are equivalent so that $\gamma_\theta = \gamma_\phi$. The growth induces an elastic deformation of the cyst characterized by the three elastic deformation gradients α_i. The total geometric deformation gradients in the 3 directions are then $\alpha_r\gamma_r$ and $\alpha_\theta\gamma_\theta = \alpha_\phi\gamma_\phi$. These deformations give the change in length of a small unit element, in direction i, of size dL_i in the reference state, which after a deformation during the time t has a size $d\ell_i = \alpha_i\gamma_i\, dL_i$.

In addition, incompressibility is generally assumed for living tissues [16], so that any volume increase or decrease is only due to the growth process and not to elasticity. This incompressibility condition imposes a relationship between the elastic stretches : $\alpha_r(\alpha_\theta)^2 = 1$. Therefore, the only remaining unknown is $\alpha = \alpha_\theta = \alpha_r^{-1/2}$. The volume change from an initial volume V_i to a volume V_f is then given by $J = V_f/V_i = \gamma_r\gamma_\theta^2$. We also define the growth anisotropy as $\gamma = \gamma_r/\gamma_\theta$. In principle, anisotropic growth reflects the internal structure of the tissue such as the fiber orientation of the cytoskeleton of the cells; but in the cyst, it may be due also to the arrangement of the cells and their interactions.

Growth of the cyst results from cell growth and division which is a discrete process, expected to be much longer than the cell rearrangement and the mechanical relaxation. In order to calculate the elastic deformations at each time, we divide the growth process into discrete time steps of duration δt which covers these three stages, and is probably of the order of magnitude of the

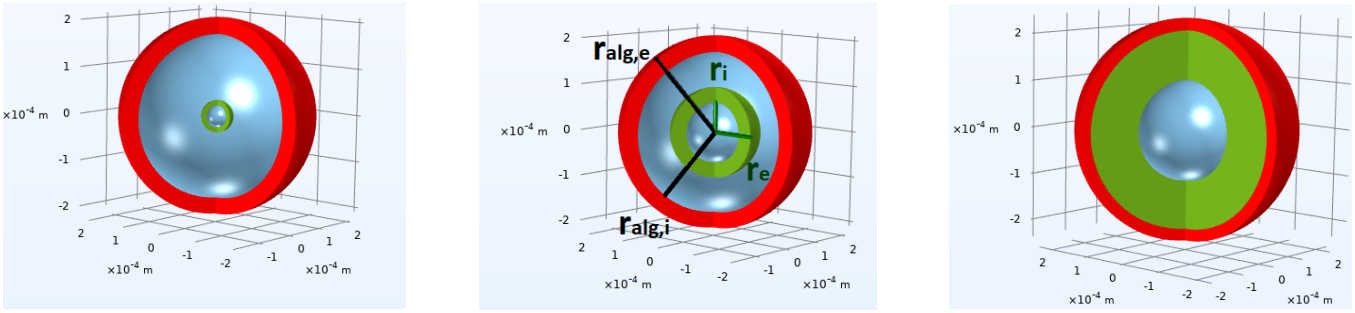

(a) (b) (c)

FIG. 3: **Sketch of the cyst-alginate system. (a) :** *at time* $t = 0$. **(b) :** *during growth in the pre-confluent stage.* **(c) :** *after confluence. The cyst is in green and the alginate in red, the blue represents the fluid between the cyst and the alginate and in the lumen.* $r_i, r_e, r_{alg,i}, r_{alg,e}$ *correspond respectively to the inner radius of the cyst, the outer radius of the cyst, the inner radius of the alginate capsule, and the outer radius of the alginate capsule.*

cell division time. The incremental growth deformation gradients during the nth time step are $\gamma_r^0(n)$ and $\gamma_\theta^0(n) = \gamma_\phi^0(n)$. At a time $t = N\delta t$, the eigen-values of the growth tensor are $\gamma_i(t) = \prod_{n=1}^{N} \gamma_i^0(n)$. The growth rates k_i in the three directions are defined as $k_i(t) = \partial_t \log \gamma_i(t)$. The total volume growth is defined as $J = \gamma_r \gamma_\theta^2$, so the volume growth rate is $k = k_r + 2k_\theta$ with a typical proliferation time $\tau = 1/k$, and a division time $\tau_d = \tau \ln(2)$. After a time $t = N\delta t$ the growth rates are related to the incremental growth deformation gradients by $k_i = k_0 \log(\gamma_i^0(N))$ where $k_0 = 1/\delta t$. If the incremental growth factors are constant in time and equal to γ_r^0 and γ_θ^0, the growth rate is constant and the growth deformation eigen-values increase exponentially with time $\gamma_i(t) = \exp(k_i t)$. In this case, using the discrete time steps, after N time steps, the growth deformation gradients at a time t are $(\gamma_r, \gamma_\theta) = ((\gamma_r^0)^N, (\gamma_\theta^0)^N)$, the growth anisotropy becomes : $\gamma(N) = (\gamma_r^0)^N/(\gamma_\theta^0)^N$ while the total volume growth amount is $J_N = \gamma_r \gamma_\theta^2 = (\gamma_r^0)^N (\gamma_\theta^0)^{2N}$. Anisotropic growth generates elastic strains and stresses [15] : this constitutes a fundamental hallmark of morpho-genesis and embryo-genesis. These quantities combined to the geometry of the tissue explain most of the shapes observed in nature such as the brain cortex [17], the intestine [18, 19], algae [20], and plants [21, 22]. Indeed, when the growth is slow enough that elasticity dominates, biological tissues deform and buckle following simple rules : their shapes minimize an elastic energy with constraints given by the boundary conditions [15, 23]. In our case, the boundary conditions impose the normal stress at the inner and outer boundaries of the cyst or at the boundary of the cyst and the capsule. In the following, we make the important assumption that the cyst and the alginate are perfectly porous to water so that any liquid flux due to geometrical changes equilibrates much faster than the growth process itself. Therefore the pressure in the fluid is constant both outside the capsule, inside the capsule and in the cyst lumen, and this constant is fixed to zero.

In the pre-confluence stage of the growth when the cyst is not yet in contact with the capsule (*Fig. 3a-3b*), the normal stress which is approximately $E_{cyst}\,\alpha \sim 10\,\text{kPa}$ (with E_{cyst} the cyst Young's modulus) must equilibrate the Laplace pressure due to the surface tension of order σ/R_i. The surface tension of an epithelium estimated from Xenopus embryonic cells [24] is of order $0.5\,\text{mN.m}^{-1}$, and the ratio between capillarity and elasticity stresses is then of order 10^{-2}. This allows to neglect the surface tension, and therefore the boundary conditions both at the inner and outer boundaries of the cyst impose that the normal stress vanishes. We then find the elastic deformation by minimization of the total elastic energy with respect to the circumferential deformation α or equivalently by writing the stress balance in the radial direction. The total elastic energy $\mathcal{E}$ is obtained by integration over the volume of the hyper-elastic energy density $\hat{W}$:

$$\mathcal{E} = 4\pi \int_{R_i}^{R_o} R^2 dR J_n \hat{W}(\alpha) \tag{1}$$

We use here a Lagrangian description and R_i and R_o are respectively the initial inner and outer radii of the cyst. In a spherical geometry, the deformation gradient is $\alpha = r/(R\gamma_\theta)$, r being the current radius of the inner sphere inside the cyst initially located at R. We choose the Neo-Hookean model for incompressible materials, which is the simplest model of hyper-elasticity both for the cyst and the alginate :

$$\hat{W}_{NH} = \frac{E}{6}(\alpha^{-4} + 2\alpha^2 - 3) \tag{2}$$

The Young modulus of the cyst E_{cyst} is smaller than the Young modulus of the alginate E_{alg}. Notice that, contrary to the cyst, the capsule does not grow so that inside the capsule $\gamma_r = \gamma_\theta = \gamma = 1$. Using the radial stress balance, we calculate the radial

Cauchy stress [15] :

$$t_r - t_i = \int_{r_i}^{r} \frac{\alpha}{r} \partial_\alpha \hat{W} dr = \int_{\alpha_i}^{\alpha} \gamma \frac{\partial_\alpha \hat{W}}{\gamma - \alpha^3} d\alpha \tag{3}$$

The explicit calculation with the Neo-Hookean model gives

$$t_r = \frac{E}{3} \left[\frac{1}{2\alpha^4} + \frac{2}{\gamma\alpha} + \frac{\left(\gamma^2 - 1\right)}{3\gamma^{4/3}} \left\{ \log\left(\frac{\alpha\left(\alpha + \gamma^{1/3}\right) + \gamma^{2/3}}{(\alpha - \gamma^{1/3})^2} \right) - 2\sqrt{3} \tan^{-1}\left(\frac{2\alpha + \gamma^{1/3}}{\sqrt{3}\gamma^{1/3}} \right) \right\} \right]_{\alpha_i}^{\alpha} \tag{4}$$

where the bracket applied to any function f is defined as $[f(\alpha)]_{\alpha_i}^{\alpha} = f(\alpha) - f(\alpha_i)$. The volume conservation imposes :

$$\alpha^3 = \gamma \left(1 - R_i^3/R^3\right) + \alpha_i^3 \, R_i^3/R^3 \tag{5}$$

Eq. 5 provides the value of the outer radius of the cyst at each step n for a given inner deformation α_i. In the pre-confluence phase of the growth (*Fig. 3a-3b*), the radial Cauchy stress at the boundaries is equal to zero and during this period, the capsule is not perturbed by the growth of the cyst. After confluence (*Fig. 3c*), the growing cyst exerts a pressure on the capsule at $R = R_o$ and the radial stress cancels at the outer surface of the capsule and the inner surface of the cyst. At the contact cyst-capsule, the radial stress is continuous.

It is well established that a feedback exists between mechanical stresses and growth of living tissues [25, 26]. Growth is generally inhibited in compression and favored in tension. This coupling between growth and mechanics may explain the decrease of the volume growth of the cyst detected in the experiments, displayed in Fig. 4a after its contact with the capsule.

We introduce the coupling between growth and stress by writing that at each time the incremental growth deformation gradients γ_r^0 and γ_θ^0, or equivalently, the growth rates k_r and k_θ are reduced by compressive stresses [27]. For the sake of simplicity, we propose a simplified theory where the incremental growth rates only depend on the stress averaged over the thickness of the cyst [28].

Our model is now applied to the 3 experimental data sets described above. It also applies to growing aggregates but in this case the perfect spheroid geometry cannot be maintained in anisotropic growth (see first equation of Eq. 3 which diverges for $r = R = 0$). However, in practice, the nutrients do not penetrate completely inside the spheroid beyond a typical length called the penetration length [29] and a necrotic core appears when the aggregate radius is larger than this penetration length l_n. The core of the aggregate no longer grows and contingently a ring of quiescent zone. With some adaptation of the growth rate, we can apply the same model with a free outer surface but with continuity of the normal stress at the inner fictitious surface given by the penetration length. Indeed, such modelling has been used in Ref.[30] to show that stresses are generated in the proliferating rim of order of the penetration length. These stresses either radial or ortho-radial are due to inhomogeneous growth which increases from the inner border of the rim to the outer border of the aggregate.

Growth of a cyst in an alginate capsule

Our mechanical model requires the knowledge of the values of the physical and biological parameters of both the cyst and the alginate capsule: the Young moduli of the cyst and of the alginate, the radial and ortho-radial growth rates, as well as the sensibility of the growth rates to stresses. Three elastic or growth parameters are unknown, the ratio between E_{alg}/E_{cyst}, γ_r^0 and γ_θ^0, but the 2 corrective factors for the growth dependence on stress are also required. We consider that the experiments provide the initial sizes with enough precision : external and internal radii of the cyst, radius and thickness of the capsule. Our analytical treatment provides explicit values of the stresses and stretches as functions of time and of the internal and external cyst radii as function of the unknowns. The comparison with the experimental measurements shown in Fig. 2 allows to infer the unknown elastic and biological parameters.

Figure 4 displays a comparison between the 3 data sets of the 3 different experiments and the theoretical curves obtained with the best choice of parameters. The agreement between theory and experiments is satisfactory. Different experiments for close but different sizes of the capsule allow to test the reproducibility of the experiments while getting an insight into the sensitivity of the fit. In all the cases, the capsule has a thickness : $\ell = 35\,\mu$m and confluence happens at $t \approx 210\,$h which corresponds to an internal radius of the alginate $R_{i,alg} = 170 \pm 10\,\mu$m. As observed in Fig. 4a, the growth rates change significantly after confluence between the cyst and the capsule. Since the dependence of the growth tensor is also a second order tensor, many formulations are then possible as discussed in the Supplementary Materials.

We choose the simplest correction for the dependence of the growth on stress: $k_\theta = k_\theta^0 + k_\theta^1 < t_r >$ and $k_r = k_r^0 + k_r^1 < t_r >$ (the more compressive the radial stress, the smaller the growth rate).

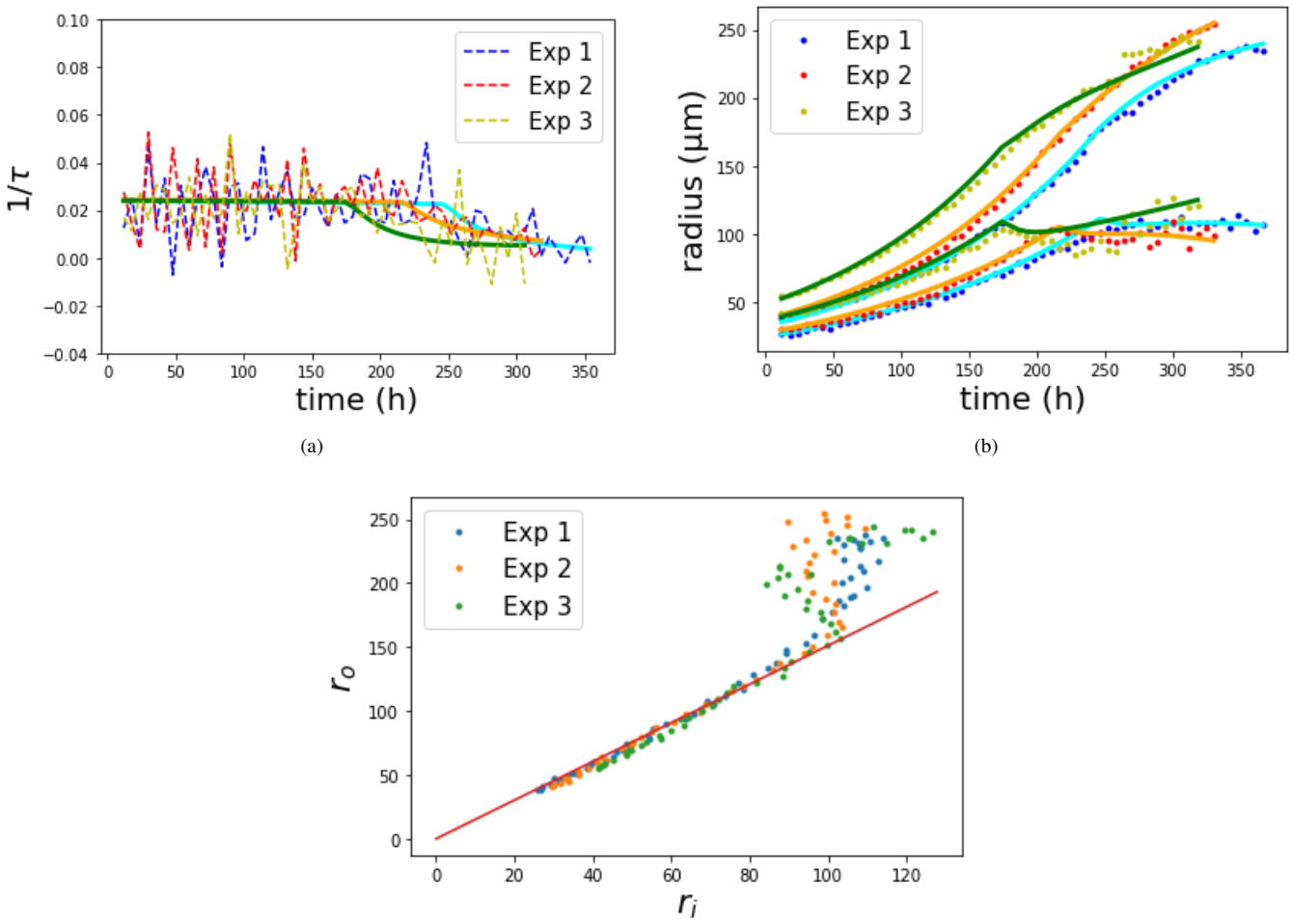

(a) (b)

(c)

FIG. 4: **Calibration of the theoretical model for 3 experiments with cells of a single cell type** *(dots and dotted lines are the experimental data, and the continuous lines are obtained by the present model).* **(a)** : *Evolution of the volume growth rates with time. Confluence does not happen at the same time for the different experiments. The value of the volume growth rate in the absence of stress is* $k_0 = 1/\tau = (2.41 \pm 0.03) \times 10^{-2}\,\mathrm{h}^{-1}$. *This corresponds to a doubling time :* $\tau_d = 28.7 \pm 0.3\,\mathrm{h}$. **(b)** : *Inner and outer radii from experimental data (dots) and theoretical curves (lines). The values of the different parameters obtained from the calibration of the theoretical model are shown for the three experiments in Table. 1.* **(c)** : *Outer radius versus inner radius. Before confluence, the relation between the outer and inner radii is almost linear due to the weak interplay between elasticity and growth :* $r_o \approx (R_o/R_i) \times r_i \approx 1.5 \times r_i$.

Experiment	Exp 1	Exp 2	Exp 3
E_{cyst} (kPa)	11.3	11.3	8.5
$k_r\ (10^{-3}\,\mathrm{h}^{-1})$	8.9	9.08	8.95
$k_\theta\ (10^{-3}\,\mathrm{h}^{-1})$	6.7	6.75	6.85
$k_r^1\ (10^{-3}\,\mathrm{h}^{-1})$	4	1	5
$k_\theta^1\ (10^{-3}\,\mathrm{h}^{-1})$	5	4.4	3

TABLE I: *Table of the free parameter values obtained from the calibration of the model for the three different experiments shown in Fig. 4.*

The growth rates are more sensitive to the radial stress t_r, than to the ortho-radial stress t_θ. This behavior can be explained by the stacking of more than one cell layer in the radial direction of the cyst.

Figure 4b displays the comparison of the theoretical results to the different sets of experimental data. We can estimate the Young moduli of the cysts in the two experiments by calibration : $E_{cyst} = 9.9 \pm 1.4\,\mathrm{kPa}$. This value is on the same order of magnitude as previous measurements on cell monolayers of MDCK cells for which the Young's modulus was $20 \pm 6\,\mathrm{kPa}$ [31]

The values obtained for k_r and k_θ are different, indicating a growth anisotropy. Nonetheless, the growth is closer to isotropic

before confluence than after confluence, resulting in a relation between r_i and r_o that is almost linear (***Fig. 4d***) since $\alpha = r/(R\gamma_\theta)$ and $\alpha^{-2} = (dr/dR)/\gamma_r$. The deformation gradient is also low before confluence (***Fig. S2a***).

Comparing the cyst growth with the growth of an aggregate of approximately the same size for the outer radius, the mathematical modeling of Ref. [30] shows that the radial stress increases from 0 to 0.8 before decreasing to -1.5 when R varies from the inner to the outer contour while the ortho-radial stress varies from 2 up to -3 in units of the cell stiffness. These changes occur when the volume increase is about two folds which is rather modest compared to our experiments. Indeed, to adapt quite exactly the numerical results obtained in Fig.1-B of Ref. [30], we must restrict to the blue curve of Fig. 4 after 90 hours approximately. We then expect that more significant growth rates will lead to stresses of order several times the Young modulus, a value much much larger than what we detect in the cyst before confluence (see Fig.S2 (b)).

Finally, another typical feature of morpho-elasticity is the surface buckling for oriented growth which occurs for large enough values of the growth elongation. Indeed, oriented growth, by boundary constraints or anisotropy, generates compressive stresses in the direction of low extension. In our case, the compressive stress is in the ortho-radial direction where $\alpha < 1$. This symmetry breaking has been first explained by Biot [32]. It is observed in Fig. (1c, 2) at the end of the experiment for $t > 315\,\mathrm{h}$. The radial Cauchy stress t_r at the interface cyste/alginate acts as a pressure $P \sim 0.4\,E_{cyst}$ applied at R_o. The growth anisotropy ratio $\gamma \sim 3$ and the inner ortho-radial elastic deformation $\alpha \sim 0.65$ point to a compressive stress on the internal surface. The surface instability, which appears on the inner cyst surface is consistent with the values of the stress found in the study of the shell bifurcation performed [15] in the case of thick shells and low number of oscillations.

Conclusion

Spontaneous PSC aggregates formed in biomedical engineering devices contrast with the self-organization of these cells reported in developmental biology. By engineering a stem cell niche within capsules loaded with very few PSCs and by imaging them over long time periods, we solve this puzzle. We find that PSCs initially form cysts that grow and thicken, become pseudo-stratified epithelia and finally fill up the whole volume of the capsule. The cyst configuration allows for the same direct access to nutrients for each cell. This is very different from what happens in cell aggregates. This leads to homogeneous growth and low elastic stresses. In general, growth inhomogeneity due to the nutrient access is a major source of stresses in volumetric growth. Since cells are not submitted to any significant mechanical constraints, they preserve their stemness and polarization. We demonstrate that stresses increase slowly during cyst evolution due to anisotropic growth effects. Late stages of growth, also associated with the contact with the capsule show larger stresses that may affect the fate of PSCs, e.g by triggering uncontrolled differentiation or inducing mutations that will affect the overall phenotypic and genotypic quality of these stem cells for applications in regenerative medicine. We speculate that optimizing the industrial production could require to reach a precise time control of the growth and to know precisely when to end the growth of the cysts before passaging them. To this end, building a minimal mechanical model that describes accurately and quantitatively the growth dynamics of these cysts will hopefully provide a predictive approach that will help to adapt the current empirical approaches.

Acknowledgements

The authors acknowledge the support of ANR (Agence Nationale de la Recherche) under the contract MecaTiss (ANR-17-CE30-0007) and Parkington (ANR-17-C18-0026-02).

Competing interests

The authors declare no competing interests.

Materials and Methods

Ethics statements

Generation, use and storage of human iPSCs were performed with approval from the “Comité de Protection des Personnes” (CPP) Ile de France (DC 2015-2595 and 2016-A00773-48).

Human pluripotent stem cell lines and culture conditions

We used a commercial hiPSC line (ThermoFisher: GibcoTM episomal hiPSC line (A18945)) generated using cord blood derived CD34+ progenitors with seven 7 episomally expressed factors (Oct4, Sox2, Klf4, Myc, Nanog, Lin28, and SV40 T). HiPSC cells were maintained on Matrigel (Corning, # 354234) and cultured in mTeSR1 medium (StemCell Technologies 85875). These 2D cell cultures were fed daily, passaged with an enzyme-free reagent, ReleSRTM (StemCell Technologies 05873) every 3-6 days (around 80% confluency) and replated as small clusters (between 100 to -and 200 µm) at a density of about $5000 - 10000\,\mathrm{cells}/\mathrm{cm}^2$. Cells were cultured at 37°C in a humidified atmosphere containing 5% CO2.

Encapsulation process

Prior to encapsulation, the 2D hiPSC colonies were detached (using ReLeaSRTM) and dissociated into a near single cell suspension using Accutase (Stem Cell Technologies 07920). HiPSCs were then mixed in a 50/50 volume ratio with Matrigel at 4°C to keep the suspension in a liquid state. The final concentration of cells in the cell/matrix solution was thus between 0.4-1.0×106 viable cells/mL, referred to as the encapsulation density. The encapsulation system is similar to the one described in [12]. In brief, ethylene tetrafluoroethylene tubings are connected to the three inlets of a 3D printed (using the DLP Micro Plus Hi-Res printer from EnvisionTEC) microfluidic co-laminar flow device. An extruded and polished glass microcapillary tip (of diameter ∼150 µm) is glued to the outlet of the nozzle for a better control of the flow. The cell/matrix suspension is loaded into the inner channel of the 3-way device, which is kept refrigerated thanks to an in-line cooling system in order to prevent premature gelation of Matrigel. A solution of sodium alginate (Novamatrix Pronova SLG100, 0,25 g #4202101 at 2% in distilled water) is injected into the outer channel. To prevent alginate gelation within the microfluidic device due to calcium release from the suspended cells, a calcium-free solution (Sorbitol 300mM, Sigma-Aldrich 85529) is used in the intermediate channel of the co-extrusion chip and serves as a barrier against calcium diffusion. Typical flow rates for the three solutions were 45mL/h, 45mL/h and 30mL/h for the alginate solution, the sorbitol solution and the cell+matrix suspension, respectively. At these rates, the composite solution forms a liquid jet that fragments into droplets (of about twice the size of the nozzle) due to the spontaneous Rayleigh-Plateau instability. To avoid subsequent coalescence of the train of droplet, an alginate charging part and a copper ring are connected to a high voltage (2000 V) generator. When the composite droplets contact the collecting calcium bath (at 100 mM), the outer alginate layer readily gelates. As a consequence, the inner cell/matrix solution remains entrapped inside a closed, spherical and permeable micro-compartment. Within 1 min following encapsulation, capsules are rinsed with medium (DMEM) to reduce the basal calcium concentration. Finally, they are transferred to the suspension culture medium, mTeSR1.

Suspension culture of hiPSC capsules

Suspension cultures of encapsulated hiPSC were carried out in T-Flasks placed in a cell culture incubator at 37°C and 5% CO2. The mTeSR1 medium was supplemented with 10 µM Y-27632 for ROCK inhibition only during the first 24 hours of culture. From culture day 3, the medium was exchanged every day as follows. The contents of the T-Flasks were transferred into Falcon Tubes. After capsules sedimentation (within a few minutes), the supernatant was removed and replenished as the capsules were transferred back into a T-Flasks. The volume of culture medium was kept constant for the first 4 days of culture (∼4x the capsules volume). Then, the volume was steadily increased every day in order to maintain a cell concentration below 106 cells/mL.

Time-lapse microscopy of encapsulated hiPSC cyst growth

Time-lapse microscopy was performed using a Nikon Biostation IM microscope with a 10x objective. Capsules containing hiPSCs were transferred to a 35 mm Petri dish 24 hours after encapsulation. Approximately 20 capsules were placed in the Petri dish containing 5 mL of fresh Y-27632-free mTeSR1 medium. Cyst growth was monitored over about 2 weeks. Practically, images were taken every 6 to 10 minutes at preselected Z-focal planes to ensure acquisition at proper focus in case of undesired drift.

Immunostaining

The alginate capsule was removed prior to fixation by incubating the samples in PBS without divalent cations for at least 5 minutes with agitation at RT. 3D hiPSC colonies were fixed with 4% PFA for 30-60 minutes at RT in the dark. The samples were then washed 3x with 0.1% Tween20 in PBS. A permeabilization step was done in parallel with excess PFA quenching in a PBS solution containing 0.3% Triton X-100 and 100 mM Glycine for 30 minutes, followed by 3x washing with 0.1% Tween20 in PBS. The samples were incubated in primary and secondary antibodies in 1% BSA + 0.1% Tween20 in PBS overnight at 4° with gentle orbital agitation, including a 3x rinsing with 1% BSA + 0.1% Tween20 in PBS after each incubation. Actin and nuclear staining were performed with Phalloidin Alexa Fluor 647 (1:500 dilution, Thermo A22287 2015553) and Hoechst 33342 (1:1000 dilution). Pluripotency maintenance was assessed by immunofluorescence staining of SOX2 and OCT4 using OCT 3/4 mouse IgG2b (1:200, Santa Cruz Biotechnology sc-5279 E1818), SOX2 rabbit polyclonal (1:1000, Sigma Aldrich AB5603 3153252), secondary donkey anti-mouse IgG H+L Alexa Fluor Plus 488 (1:500, Thermo/Invitrogen A32766 TF271737A), secondary donkey anti-rabbit IgG H+L Alexa Fluor Plus 555 (1:500, Thermo/Invitrogen A32794 TH271030). Samples were imaged on either a Leica SP5 or SP8 confocal microscope (Bordeaux Imaging Center, BIC).

Image analysis

Image analysis was performed using ImageJ. The external and internal effective radii of the cysts, r_o and r_i, were measured from the equatorial corresponding cross sections S according to $r_{o,i} = (S_{o,i}/\pi)^{1/2}$ after applying appropriate bandpass filters and thresholds. The thickness h of the cyst was derived from $h = r_o - r_i$ and the volume V of the epithelium was calculated as $V = 4\pi(r_o^3 - r_i^3)/3$.

Supplementary Materials

Mechanical model

To obtain the inner and outer radii of the cyst in the current state, we assume that the pressures inside the lumen and in the outer medium vanish, and we solve the equation for the stress at the outer boundary Eq. 3:

$$0 = \int_{\alpha_i}^{\alpha_o(\alpha_i)} \gamma \frac{\partial_\alpha W}{\gamma - \alpha^3} d\alpha + \int_{\alpha_{i,alg}(\alpha_i)}^{\alpha_{o,alg}(\alpha_i)} \frac{\partial_\alpha W}{1 - \alpha^3} d\alpha \tag{S1}$$

where we have separated the contributions from the cyst and the capsule and where the unknown is α_i. $W = E/6(\alpha^{-4}+2\alpha^2-3)$, α is the angular elastic deformation, α_i is the value of this deformation taken at the inner surface of the cyst, α_o the deformation of the cyst at the interface between the cyst and the alginate, $\alpha_{i,alg}$ the deformation at the inner surface of the alginate, and $\alpha_{o,alg}$ the deformation at its outer surface. All these deformations can be written as functions of α_i using volume conservation (*Eq. (5)*). Before confluence, the deformation is $\alpha = 1$ in the alginate and the second integral cancels. Eq. (S1) provides the value of α_i. Knowing the growth deformation γ_θ, we can calculate the inner radius in the current state $r_i = \alpha_i \gamma_\theta R_i$ using the radius R_i in the reference state. Volume conservation then yields the value of the outer radius.

The total growth deformations $\gamma_\theta(t_n), \gamma_r(t_n)$ at step n which correspond to a time $t = n\delta t$ are the products of the incremental growth deformations $\gamma_\theta^0(t_i), \gamma_r^0(t_i)$ so that : $\gamma_\theta(t_n) = \Pi_{i=1}^n \gamma_\theta^0(t_i), \gamma_r(t_n) = \Pi_{i=1}^n \gamma_r^0(t_i)$ with $\gamma_r^0(t_i) = \mathrm{e}^{k_r(t_i)\delta t}, \gamma_\theta^0(t_i) = \mathrm{e}^{k_\theta(t_i)\delta t}$. The angular and radial growth rates are linear functions of the mean radial stress in the cyst : $k_\theta = k_\theta^0 + k_\theta^1 < t_r >$ and $k_r = k_r^0 + k_r^1 < t_r >$ where $< t_r >= 3\int_{r_i}^{r_o} r^2 t_r dr/(r_o^3 - r_i^3)$. The stress at radius r in the current state which corresponds to the radius R in the initial configuration in the cyst is given by the relation :

$$t_r = \int_{\alpha_i}^{\alpha(\alpha_i)} \gamma \frac{\partial_\alpha W}{\gamma - \alpha^3} d\alpha \tag{S2}$$

where α in function of R and α_i is given by volume conservation (Eq. 5).

Other models of the time evolution of the growth rates with time can be tested, but yield less satisfactory results. The first option is to consider constant growth rates : $k_\theta = k_\theta^0$, $k_r = k_r^0$. A refined possibility is a linear dependence of the growth rates on average pressure $k_\theta = k_\theta^0 + k_\theta^1 < P >$, $k_r = k_r^0 + k_r^1 < P >$. This last possibility yields a rather good description of the experiments but at long times, the total volume growth J reaches a plateau, whereas in the experiments it continues to decrease. The results are shown in Fig. S1. We therefore choose a variation of the growth rates with the radial stress that leads to a decrease of the growth rates for the whole duration of the confluence stage (Fig. S2c).

An error ϵ to quantify the adequacy of the theoretical model to the experiments is calculated as follows :

$$\epsilon = \frac{1}{3}\sum_{j=1}^{3} \frac{1}{2\mathcal{N}_j} \sqrt{\sum_{k=1}^{\mathcal{N}_j} \left[\left(r_{j,k}^{th,o} - r_{j,k}^{exp,o} \right)^2 + \left(r_{j,k}^{th,i} - r_{j,k}^{exp,i} \right)^2 \right]} \tag{S3}$$

where j is the number of the experiment (Exp 1-2-3), $\mathcal{N}_j$ is the number of experimental points in this experiment. There are $\mathcal{N}_j$ experimental points indexed by j, k for the outer radius of the cyst $r_{j,k}^{exp,o}$, and $\mathcal{N}_j$ experimental points for the inner radius of the cyst $r_{j,k}^{exp,i}$. Those points correspond to the points $r_{j,k}^{th,o}$ and $r_{j,k}^{th,i}$ in the theoretical model.

Fig. S2c-S2d display the evolution of the global growth rates with time. A discontinuity appears at confluence,with a significant change in the growth rates. Fig. S2a-S2b show the evolution with time of the angular elastic deformation at the interface between the cyst and the lumen, the radial stress taken at the interface between the cyst and the lumen and the averaged radial stress in the cyst. These values justify the observation of the buckling instability at the end of the experiment.

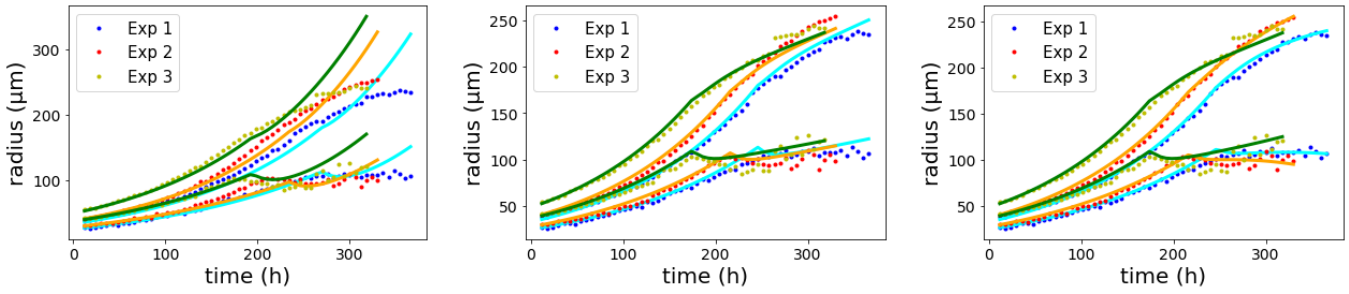

(a) (b) (c)

FIG. S1: *Cyst radii and calibration of the growth rates according to the model.* **(a) :** The growth rates are constant in time : $\epsilon = 3.12$. **(b) :** The growth rates depend on the averaged pressure in the cyst : $\epsilon = 1.13$. **(c) :** The growth rates have a linear dependence on the averaged radial stress in the cyst : $\epsilon = 0.80$.

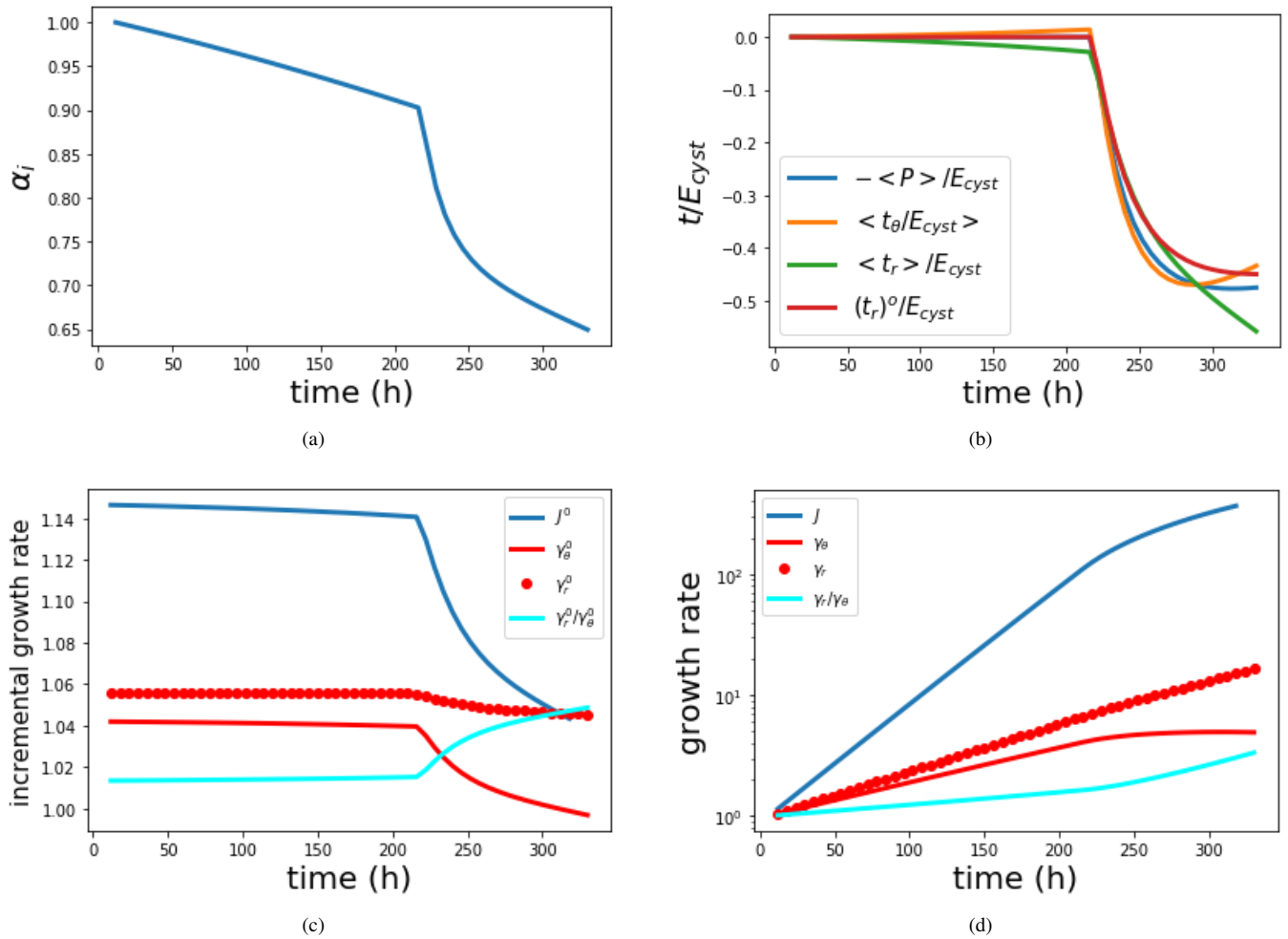

(a) (b) (c) (d)

FIG. S2: *Time evolution of several computed quantities in Experiment 2.* **(a) :** *Evolution of the angular elastic deformation gradient at the inner surface of the cyst* α_i. ***(b) :*** *The mean radial, the ortho-radial stresses and the stress invariant* $< t_r >, < t_\theta >, - < P >$ *as well as the radial stress at the outer surface* $(t_r)_o$ *normalized by* E_{cyst}. *Those values contribute to explain the buckling instability at the end of the experiment.* **(c,d) :** *Evolution of the different incremental (c) and total (d) growth variables* $J = \gamma_\theta^2 \gamma_r, \gamma_\theta, \gamma_r, \gamma = \gamma_r/\gamma_\theta$ *with time.*

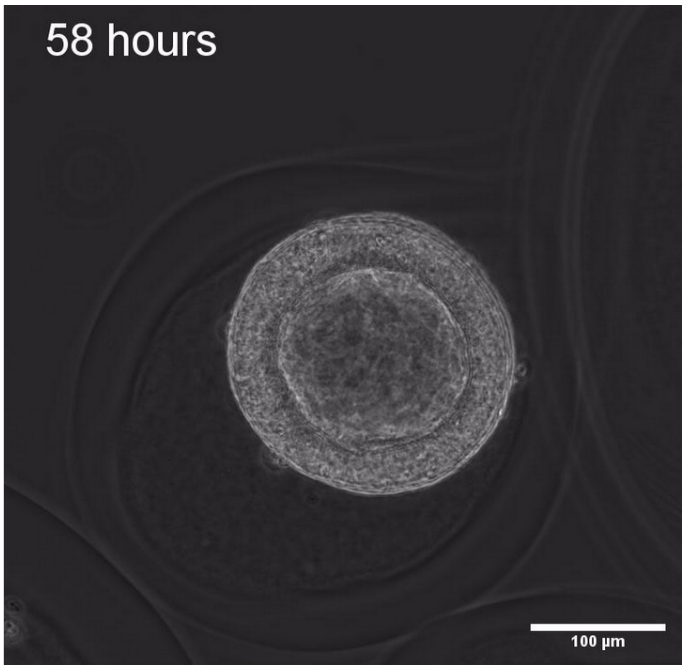

Movie S1: **Movie displaying the full process of the growth during the pre-confluence and the post-confluence stages.** *The link to access the movie is :* https://documentcloud.adobe.com/link/track?uri=urn:aaid:scds:US:f5a2b14a-d1cc-48f0-b952-b4d40e99910b#pageNum=1.

* Corresponding author. Email : benamar@lps.ens.fr

[1] Kazutoshi Takahashi and Shinya Yamanaka. Induction of pluripotent stem cells from mouse embryonic and adult fibroblast cultures by defined factors. *cell*, **126**(4):663–676, 2006.

[2] Jo'an Bardy, Allen K Chen, Yu Ming Lim, Selena Wu, Shunhui Wei, Han Weiping, Ken Chan, Shaul Reuveny, and Steve KW Oh. Microcarrier suspension cultures for high-density expansion and differentiation of human pluripotent stem cells to neural progenitor cells. *Tissue Engineering Part C: Methods*, **19**(2):166–180, 2013.

[3] Breanna S Borys, Tania So, James Colter, Tiffany Dang, Erin L Roberts, Tamas Revay, Leila Larijani, Roman Krawetz, Ian Lewis, Bob Argiropoulos, et al. Optimized serial expansion of human induced pluripotent stem cells using low-density inoculation to generate clinically relevant quantities in vertical-wheel bioreactors. *Stem Cells Translational Medicine*, 2020.

[4] Yuguo Lei and David V Schaffer. A fully defined and scalable 3d culture system for human pluripotent stem cell expansion and differentiation. *Proceedings of the National Academy of Sciences*, **110**(52):E5039–E5048, 2013.

[5] Elena Garreta, Patricia Prado, Carolina Tarantino, Roger Oria, Lucia Fanlo, Elisa Martí, Dobryna Zalvidea, Xavier Trepat, Pere Roca-Cusachs, Aleix Gavaldà-Navarro, et al. Fine tuning the extracellular environment accelerates the derivation of kidney organoids from human pluripotent stem cells. *Nature materials*, **18**(4):397–405, 2019.

[6] Yue Shao, Kenichiro Taniguchi, Katherine Gurdziel, Ryan F Townshend, Xufeng Xue, Koh Meng Aw Yong, Jianming Sang, Jason R Spence, Deborah L Gumucio, and Jianping Fu. Self-organized amniogenesis by human pluripotent stem cells in a biomimetic implantation-like niche. *Nature materials*, **16**(4):419–425, 2017.

[7] Yi Zheng, Xufeng Xue, Yue Shao, Sicong Wang, Sajedeh Nasr Esfahani, Zida Li, Jonathon M Muncie, Johnathon N Lakins, Valerie M Weaver, Deborah L Gumucio, et al. Controlled modelling of human epiblast and amnion development using stem cells. *Nature*, **573** (7774):421–425, 2019.

[8] Kenichiro Taniguchi, Yue Shao, Ryan F Townshend, Yu-Hwai Tsai, Cynthia J DeLong, Shawn A Lopez, Srimonta Gayen, Andrew M Freddo, Deming J Chue, Dennis J Thomas, et al. Lumen formation is an intrinsic property of isolated human pluripotent stem cells. *Stem Cell Reports*, **5**(6):954–962, 2015.

[9] Kenichiro Taniguchi, Yue Shao, Ryan F Townshend, Chari L Cortez, Clair E Harris, Sasha Meshinchi, Sundeep Kalantry, Jianping Fu, K Sue O'Shea, and Deborah L Gumucio. An apicosome initiates self-organizing morphogenesis of human pluripotent stem cells. *Journal of Cell Biology*, **216**(12):3981–3990, 2017.

[10] Ruth Olmer, Alexandra Haase, Sylvia Merkert, Wei Cui, Jiří Paleček, Chen Ran, Andreas Kirschning, Thomas Scheper, Silke Glage, Konstantin Miller, et al. Long term expansion of undifferentiated human ips and es cells in suspension culture using a defined medium. *Stem cell research*, **5**(1):51–64, 2010.

[11] Kévin Alessandri, Bibhu Ranjan Sarangi, Vasily Valérïévitch Gurchenkov, Bidisha Sinha, Tobias Reinhold Kießling, Luc Fetler, Felix Rico, Simon Scheuring, Christophe Lamaze, Anthony Simon, et al. Cellular capsules as a tool for multicellular spheroid production and

for investigating the mechanics of tumor progression in vitro. *Proceedings of the National Academy of Sciences*, **110**(37):14843–14848, 2013.

[12] Kevin Alessandri, Maxime Feyeux, Basile Gurchenkov, Christophe Delgado, Anastasiya Trushko, Karl-Heinz Krause, Daniela Vignjević, Pierre Nassoy, and Aurélien Roux. A 3d printed microfluidic device for production of functionalized hydrogel microcapsules for culture and differentiation of human neuronal stem cells (hnsc). *Lab on a Chip*, **16**(9):1593–1604, 2016.

[13] Anastasiya Trushko, Ilaria Di Meglio, Aziza Merzouki, Carles Blanch-Mercader, Shada Abuhattum, Jochen Guck, Kevin Alessandri, Pierre Nassoy, Karsten Kruse, Bastien Chopard, et al. Buckling of an epithelium growing under spherical confinement. *Developmental cell*, **54**(5):655–668, 2020.

[14] Sharona Even-Ram, Vira Artym, and Kenneth M Yamada. Matrix control of stem cell fate. *Cell*, **126**(4):645–647, 2006.

[15] Martine Ben Ben Amar and Alain Goriely. Growth and instability in elastic tissues. *Journal of the Mechanics and Physics of Solids*, **53** (10):2284–2319, 2005.

[16] Pei-Hsun Wu, Dikla Raz-Ben Aroush, Atef Asnacios, Wei-Chiang Chen, Maxim E Dokukin, Bryant L Doss, Pauline Durand-Smet, Andrew Ekpenyong, Jochen Guck, Nataliia V Guz, et al. A comparison of methods to assess cell mechanical properties. *Nature methods*, **15**:491–498, 2018.

[17] Silvia Budday, Richard Nay, Rijk de Rooij, Paul Steinmann, Thomas Wyrobek, Timothy C Ovaert, and Ellen Kuhl. Mechanical properties of gray and white matter brain tissue by indentation. *Journal of the mechanical behavior of biomedical materials*, **46**:318–330, 2015.

[18] Martine Ben Amar and Fei Jia. Anisotropic growth shapes intestinal tissues during embryogenesis. *Proceedings of the National Academy of Sciences*, **110**(26):10525–10530, 2013.

[19] Edouard Hannezo, Jacques Prost, and Jean-François Joanny. Mechanical instabilities of biological tubes. *Physical review letters*, **109**(1): 018101, 2012.

[20] Kyle A Serikawa and Dina F Mandoli. An analysis of morphogenesis of the reproductive whorl of acetabularia acetabulum. *Planta*, **207** (1):96–104, 1998.

[21] Karen Alim, Shahaf Armon, Boris I Shraiman, and Arezki Boudaoud. Leaf growth is conformal. *Physical biology*, **13**(5):05LT01, 2016.

[22] Fan Xu, Chenbo Fu, and Yifan Yang. Water affects morphogenesis of growing aquatic plant leaves. *Physical review letters*, **124**(3): 038003, 2020.

[23] Alain Goriely. *The mathematics and mechanics of biological growth*, volume 45. Springer, 2017.

[24] Olivia Luu, Robert David, Hiromasa Ninomiya, and Rudolf Winklbauer. Large-scale mechanical properties of xenopus embryonic epithelium. *Proceedings of the National Academy of Sciences*, **108**(10):4000–4005, 2011.

[25] JD Humphrey. Vascular adaptation and mechanical homeostasis at tissue, cellular, and sub-cellular levels. *Cell biochemistry and biophysics*, **50**(2):53–78, 2008.

[26] Larry A Taber and Jay D Humphrey. Stress-modulated growth, residual stress, and vascular heterogeneity. *J. Biomech. Eng.*, **123**(6): 528–535, 2001.

[27] Robert Kiss, Henry Bock, Steve Pells, Elisabetta Canetta, Ashok K Adya, Andrew J Moore, Paul De Sousa, and Nicholas A Willoughby. Elasticity of human embryonic stem cells as determined by atomic force microscopy. *Journal of biomechanical engineering*, **133**(10), 2011.

[28] Alain Goriely and Martine Ben Amar. On the definition and modeling of incremental, cumulative, and continuous growth laws in morphoelasticity. *Biomechanics and modeling in mechanobiology*, **6**(5):289–296, 2007.

[29] Joseph Ackermann, Martine Ben Amar, and Joanny Jean-François. Multi-cellular aggregates, a model for living matter. *ENS preprint, to appear*, 1–53, 2021.

[30] Alain Goriely and Martine Ben Amar. Differential growth and instability in elastic shells. *Physical review letters*, **94**(19):198103, 2005.

[31] Andrew R Harris and GT Charras. Experimental validation of atomic force microscopy-based cell elasticity measurements. *Nanotechnology*, 22(34):345102, 2011.

[32] Maurice A Biot. Surface instability of rubber in compression. *Applied Scientific Research, Section A*, **12**(2):168–182, 1963.